GEOLOGICA CARPATHICA, 51, 4, BRATISLAVA, AUGUST 2000
265–278

PERMIAN LACUSTRINE PHOSPHATIC SANDSTONE IN THE SOUTHERN GEMERIC UNIT, WESTERN CARPATHIANS, SLOVAKIA

ANNA VOZÁROVÁ and IGOR ROJKOVIČ

Faculty of Science, Comenius University, Mlynská dolina, 842 15 Bratislava, Slovak Republic

(Manuscript received November 20, 1999; accepted in revised form March 15, 2000)

Abstract: Lenses of phosphatic sandstone occurring in the Permian sediments of the Štítnik Formation contain intraclasts of microsphorite as well as minute apatite crystals in the matrix. The microsphorite is composed of pelmicritic and microsparitic aggregates of fluorapatite. The sandstone contains up to 18 weight percent P_2O_5. The phosphatic sandstone originated in an eutrophic lacustrine environment as a result of phosphorus concentration in lake sediment due to the iron redox cycling and the associated microbiological effects. Two contrasted depositional realms are suggested: 1. a shallow, lacustrine low-energy depositional regime in which adsorption and desorption of iron-bound phosphorus between oxygen-deficient bottom water and anoxic sediment led to the formation of microsphorite deposit; 2. a relatively high-energy depositional regime during which river deltas invaded the lacustrine environment and affected phosphorite reworking. Apatite crystals in the matrix are accompanied by Fe-dolomite, uraninite, U-Ti oxides, Ti oxides, framboidal pyrite, chlorites, muscovite and albite. Their formation reflects diagenetic to very low-grade metamorphic redistribution. A hydrothermal association of minerals represents sulphide mineralization occurring in quartz-carbonate veinlets.

Key words: Western Carpathians, Permian, lacustrine phosphorite, mineral composition, REE, diagenesis, metamorphism.

Introduction

The Permian sequences in the Western Carpathians are dominated by continental, mainly coarse-grained "red-beds" sedimentary formations. Their origin was related to a transpressional and extensional tectonic regime. Therefore, the occurrence of phosphatic sandstone in the Permian sequence of the Southern Gemeric Unit is unique, compared to other Permian sediments in the Western Carpathians. Phosphatic sandstone forms thin lenses (0.2 to 0.4 m thick; 2 to 6 m long, max. 2 m wide) within the relatively monotonous sandy-shaly complex of the Štítnik Formation. The Southern Gemeric Permian deposits show a peculiar geodynamic position. They represent the post-collisional sequence with respect to the Hercynian orogeny that prograded to the initial stage of the Alpine orogeny.

The sedimentary complex of the Štítnik Formation was first described as a "marine Permian facies" (Bystrický & Fusán 1955). The first finding of phosphatic sandstone was mentioned as marine (Tréger 1973). However, detailed lithofacies analysis suggests a continental origin for this sedimentary complex (Vozárová & Vozár 1988), though the origin of the phosphatic sandstone has not been explained satisfactorily. This paper attempts to elucidate the origin of the Permian phosphate-bearing facies on the basis of detailed geological, petrological, and geochemical analysis.

Geological setting

The Permian rocks in the Southern Gemeric Unit are classified into the Gočaltovo Group which represents a Late Hercynian post-orogenic sequence (Fig. 1). The sequence consists mostly of continental volcano-sedimentary and terrigenous rocks that grade upwards into near-shore sabkha-lagoonal facies. The basal conglomerates of Gočaltovo Group unconformably overlie the Early Paleozoic basement of the Southern Gemeric Unit, the latter is represented by flysch sediments of the Gelnica Group and Štós Formation (Vozárová & Vozár 1988). Maheľ (1986) places the Gočaltovo Group into the Meliata Unit of the Inner Western Carpathians. However, this interpretation is not supported by geological data, as the rocks of the Meliata Unit thrust over the Early Paleozoic as well as over the Late Paleozoic rocks of the Southern Gemeric Unit. Moreover, the Meliata Unit is rootless in the present Alpine structure. On the other hand, a paleogeographical relationship to Early Paleozoic basement can not be excluded due to the character of clastic detritus.

The Gočaltovo Group (Vozárová & Reichwalder in Bajaník et al. 1981) is divided into the lower Rožňava Formation and the upper Štítnik Formation (Fig. 2A).

The Rožňava Formation is represented by oligomictic metaconglomerate in the lower part and by alternating metaconglomerates, quartzose metasandstones and sandy shales in the upper part. The whole sequence shows mineral maturity, though it is structurally immature. It represents continental alluvial sediments with channel facies prevailing over sheet-flood facies. The Rožňava Formation contains two distinct horizons of metaconglomerates associated with volcanogenic horizons. The lower horizon is composed of quartz detritus and fragments of quartzose metagreywacke, with subordinate fragments of quartz-muscovite phyllite and porphyroide. This horizon is overlain by rhyolite pyroclastics (5 to 20 m thick) and, in places, by rhyodacite flows. The upper

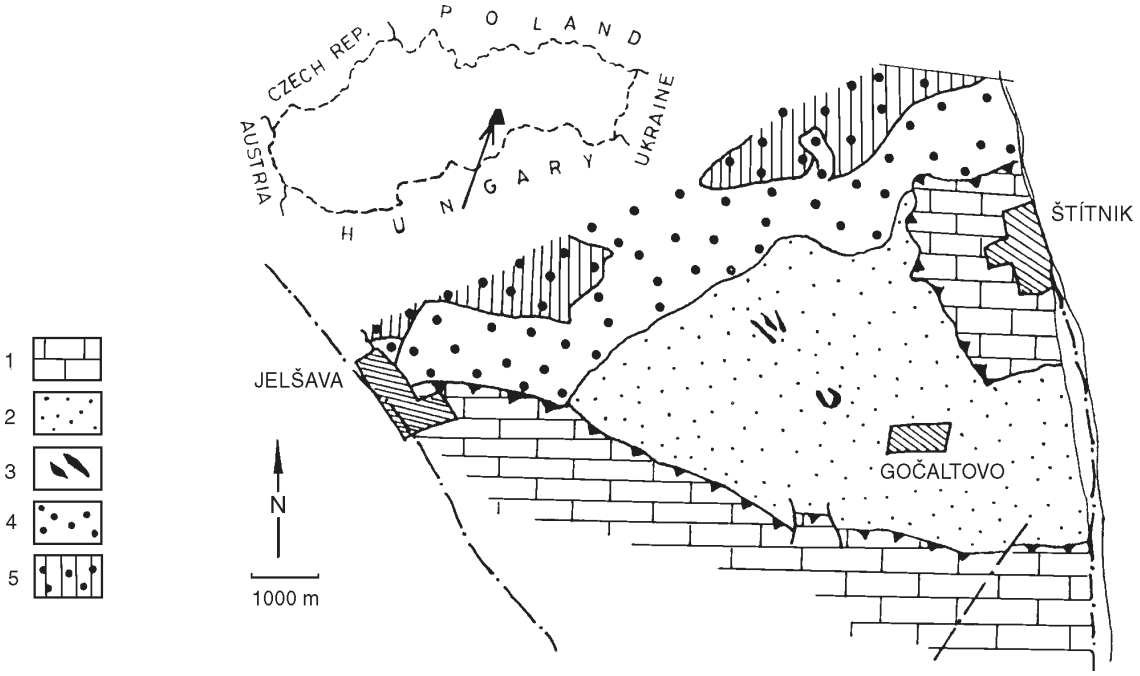

Fig. 1. Geological map of the Gočaltovo area (after Mello et al. 1996 adopted). *Explanations:* **1** — Mesozoic rock complexes of Turnaic and Meliatic units. **2–4** — Permian of the Southern Gemeric Unit: 2 — sediments of the Štítnik Formation, 3 — horizons of phosphatic sediments 4 — sediments of the Rožňava Formation. **5** — Early Paleozoic rocks of the Southern Gemeric Unit (Gelnica Group).

horizon of metaconglomerate consists of quartz pebbles and volcaniclastic material. This material bears calc-alkaline rhyolite-dacite characteristics with dominant subaeric pyroclastics. The Lower Permian age of the Rožňava Formation sediments has been documented by the presence of microflora (Planderová 1980), especially by genera *Potonieisporites*, *Striatodisaccites* and *Vittatina*.

The highly deformed rocks of the Bôrka Nappe (Mello et al. 1997, 1998) are lithologically similar to the Rožňava Formation. The oligomictic metaconglomerate, metasandstone and phyllite showing a subordinate contribution of rhyodacite volcanic rocks correspond to the Jasov Formation ("the Jasov development" according to Reichwalder 1973). The rhyodacite volcaniclastic sequence with subordinate clastic sediments is classified into the Bučina Formation (former "Bučina Beds", Fusán 1959).

The Štítnik Formation consists of alternating sandstone, siltstone and shale arranged in cyclic sedimentary sequences. It also comprises horizons of redeposited acidic volcaniclastic material. The lower part of the Štítnik Formation shows an abundance of this material, and contains irregular lenses and laminae of albite. The concentration of albite in these lenses is so high that the rock attains the albitolite character. The sequence is interpreted as having been deposited in alkaline lakes, where zeolitization of rhyolite detritus occurred, and was followed by the transformation of zeolites to albite (Vozárová & Vozár 1988). Calcitized dolostone ("dedolomite") represents the upper part of the Štítnik Formation. Calcite pseudomorphs after dolomite crystals and minute relics of dolomite enclosed in calcite indicate a dedolomitization process (Mišík, pers. commun.). These sediments overlie lenses of phosphatic sandstone (Tréger 1973). The sequence with phosphatic sandstones represents interfingering of fine-grained lacustrine sediments and fluvial sandstones. In the uppermost part of the sequence homogeneous fine-grained sediments alternate with massive sandstones and with sandstones showing graded bedding (Fig. 2B). Finely laminated shales and siltstones, commonly interlayered with thin turbiditic sandstones represent the lacustrine part of the sequence. Facies changes are abrupt between fluvial distributary sandstones and channel fill facies.

Three types of bedding structures were recognized in the sandstones:

1. graded bedding which begins with coarse grains at the base, gradually becoming finer upwards;
2. horizontal bedding marked by alternating layers of different grain size (parting-linneation);
3. sandy turbidites rich in microsphorite intraclasts.

These facies correspond to the distal river delta association interfingering with the lacustrine association. The lacustrine association is characterized by alternation of very fine-grained, laminated sandstones, siltstones and shales. It indicates still water conditions, locally interrupted by influx of thin turbidites.

Shale sequences in the Štítnik Formation contain siderite concretions and to a lesser extent quartz-barite, magnetite-hematite and pyrite concretions showing compositional similarities to hydrothermal vein deposits noted in the area (Miškovic & Varček 1983; Turan & Vančová 1983).

The carbonate and phosphate-bearing sediments as well as the hosting sandstone and shale sequences contain no fossils. Only the uppermost part of the Štítnik Formation was paleon-

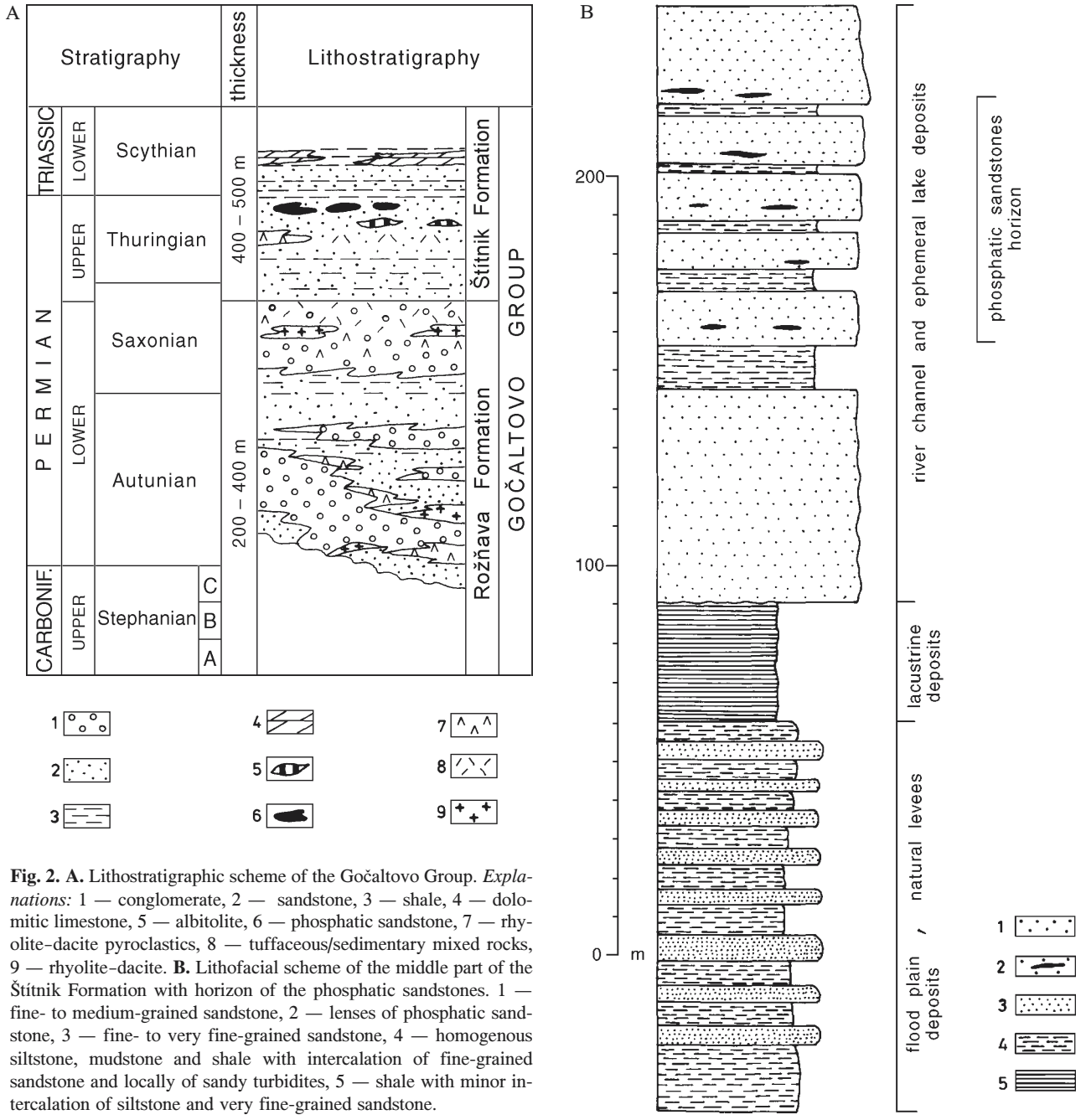

Fig. 2. A. Lithostratigraphic scheme of the Gočaltovo Group. *Explanations:* 1 — conglomerate, 2 — sandstone, 3 — shale, 4 — dolomitic limestone, 5 — albitolite, 6 — phosphatic sandstone, 7 — rhyolite–dacite pyroclastics, 8 — tuffaceous/sedimentary mixed rocks, 9 — rhyolite–dacite. **B.** Lithofacial scheme of the middle part of the Štítnik Formation with horizon of the phosphatic sandstones. 1 — fine- to medium-grained sandstone, 2 — lenses of phosphatic sandstone, 3 — fine- to very fine-grained sandstone, 4 — homogenous siltstone, mudstone and shale with intercalation of fine-grained sandstone and locally of sandy turbidites, 5 — shale with minor intercalation of siltstone and very fine-grained sandstone.

tologically dated (hill Háj, 1.5 km E from Gočaltovo village — Šuf 1963). Němejc (in Šuf 1963) reported the Upper Permian *Pseudovoltzia liebeana* (Gein) Florin and *Sphenozamites* from that part of the formation. Šuf (1963) has also found the Upper Permian *Carbonicola* McCoy 1855.

Uranium bearing sandstone with sulphide mineralization occurs in the Štítnik Formation and crops out on the slopes of Kopané and Stará hora hills 2 km W from Gočaltovo (Fig. 1). This mineralization is associated with phosphatic sandstone and occurs in banded lenses 0.2 to 0.4 m thick and 2 to 5 m long (Tréger 1973). The lenses tend to concentrate in a horizon which is up to 60 m thick (Štimmel 1967). Melnikova (1974) found that the content of P_2O_5 is up to 33 weight percent (average content at about 11 %). Our samples gave P_2O_5 up to 18 % (Rojkovič et al. 1989a).

Petrology of phosphatic sandstone

The sequence consists of alternating sandstone with pressure oriented psammitic and aleuropsammitic texture and illite-muscovite shale. The sandstone is fine- to medium-grained, with grain size ranging from 0.06 to 0.2 mm (Figs. 3, 4). Microsphorite intraclasts and carbonate concretions occur in sandstone in the Kopané hill (Figs. 5–11). Clastic grains are angular or slightly rounded and moderately sorted. Sorting

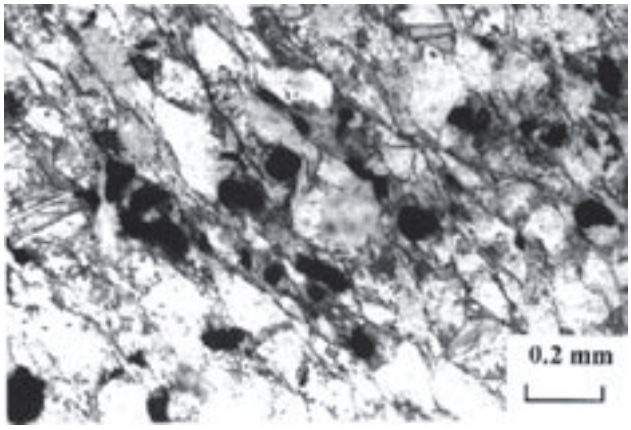

Fig. 3. Sandstone with a thin layer of heavy minerals represented by zircon (grey) and ore minerals, mainly U-Ti oxides (black). Go 7, transmitted light, parallel polar.

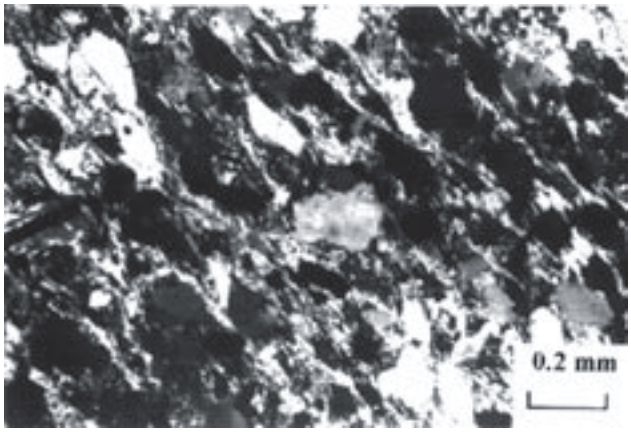

Fig. 4. Sandstone with the thin layer of heavy minerals from Fig. 3. Clastic grains of quartz, feldspars and especially sericite in the matrix (white scales) are oriented transversally to the thin layer of heavy minerals. Go 7, transmitted light, crossed polars.

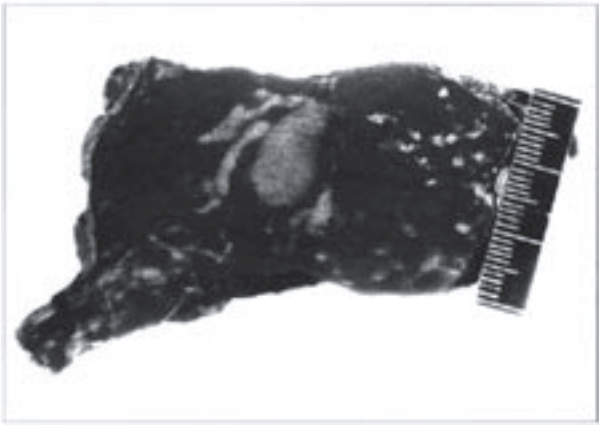

Fig. 5. Sandstone with oval and lobed intraclasts of the phosphorites (grey) and larger oval concretion of carbonate (light grey). Go 21.

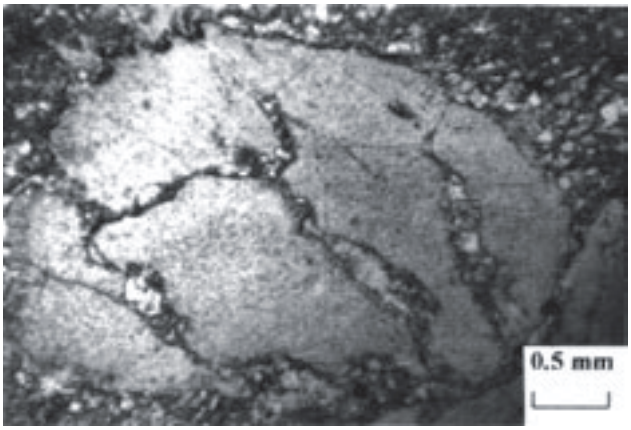

Fig. 6. Oval intraclast of phosphorite (light grey) with carbonate veinlets (white) in the sandstone. Go 21, transmitted light, parallel polar.

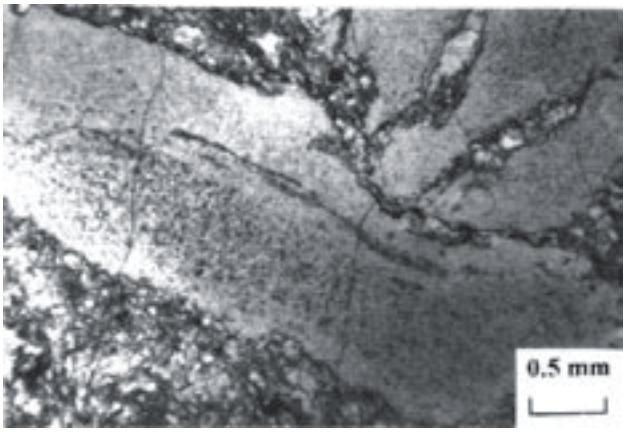

Fig. 7. Elongated intraclast of phosphorite (light grey) with oriented inclusions of quartz grains (dark grey) smaller than clastic grains of quartz in the sandstone. Go 21, transmitted light, parallel polar.

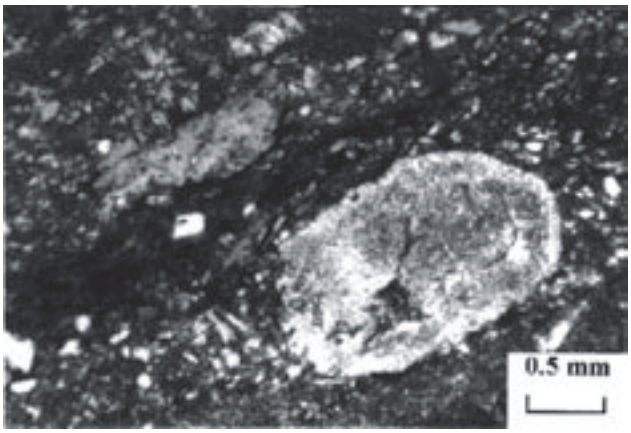

Fig. 8. Oval intraclast of phosphorite (light grey) with chlorite veinlet (dark grey transversal in centre) in the sandstone. Go 3/1, transmitted light, parallel polar.

varies from 1.0 to 0.5 φ according to visual scale of Folk (1974). The sandstone is finely laminated. The lamination consists of the alternation of laminae (parting lamination) composed of grains of two different size classes (0.1 to 0.2 mm and 0.05 to 0.1 mm). Quartz is a dominant clastic mineral. It is mostly of monocrystalline type and part of it is of volcanic

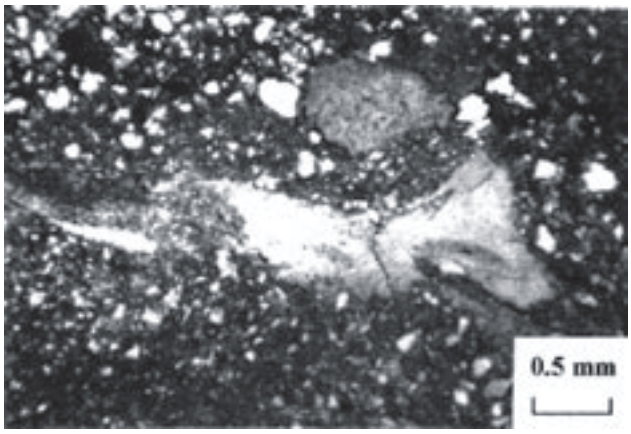

Fig. 9. Oval and elongated intraclasts of phosphorite (light grey) in the sandstone with clastic quartz grains (white). Go 4/1, transmitted light, parallel polar.

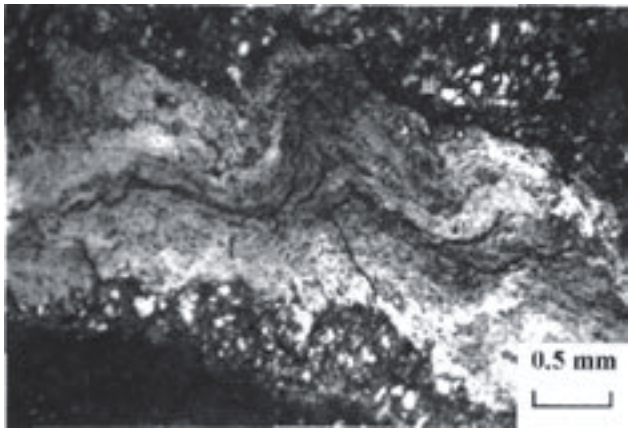

Fig. 10. Folded plastically deformed intraclast of phosphorite (light grey) in the sandstone with clastic quartz grains (white). Go 1/1, transmitted light, parallel polar.

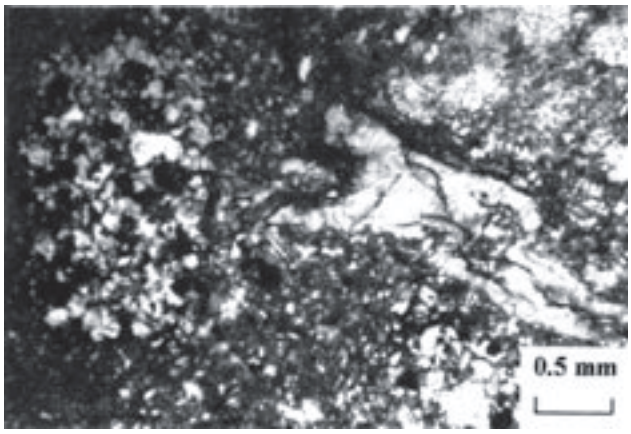

Fig. 11. Oval aggregate of albite (in left) and elongated deformed intraclast of phosphorite (light grey) in the sandstone. Go 3/2, transmitted light, parallel polar.

origin. Clastic muscovite and chloritized biotite are less common. Scarce plagioclase grains of albite-oligoclase composition and up to 0.3 mm in size are noted. The sandstone also contains shale intraclasts (up to 4 mm in diameter). Zircon occurs as rounded grains as well as prismatic crystals (up to 40 μm long) that are disseminated in the matrix. However, heavy minerals, like zircon and ore minerals (grains up to 50 μm, rarely up to 0.1 mm), are also concentrated along the horizontal lamination of the sandstone (Figs. 3–4).

The fabric of the sediment is slightly pressure-deformed, and the minerals show common recrystallization features. Elongated quartz grains are preferentially oriented parallel to the strips of white micas (Figs. 3–4). They are often slightly recrystallized, mainly at the margins and along internal fracture systems. The matrix of the sandstone consists of aggregates of white mica associated with chlorite, apatite and carbonate, with subordinate amounts of albite and fine-grained quartz. Strips of phyllosilicates are deformed by crenulation cleavage. In general, muscovite prevails over chlorite, and it is also more abundant in fine-grained sandstone. Chlorite (from 0.1 to 0.2 mm) occurs in the form of disseminated scales or sheets which alternate with muscovite. Tourmaline is not oriented (grains from 0.01 to 0.1 mm). Ore minerals are mostly disseminated in the sandstone (grains from 10 to 50 μm, rarely up to 0.1 mm in size). They also form veinlets. Fine-grained sandstone is accompanied by shale. The shale shows lepidoblastic structure, and is dominated by muscovite, with subordinate contribution of chlorite, quartz, carbonates and ore minerals.

Mineralogy of phosphatic sandstone

There are two forms of apatite in the phosphatic sandstone:

a) Oval (Figs. 5–11), irregular elongated and lobed intraclasts (mostly from 1 to 5 mm in size), which are mostly subanisotropic in polarising light. Weak anisotropy of the interlocking apatite ground-mass can be observed under high magnification.

b) Small crystals (from 5 to 20 μm in size) in the sandstone matrix (Figs. 12–13).

Microsphorite intraclasts are deformed and oriented parallel to phyllosilicate layers in the matrix. They contain carbonate veinlets as well as fragments of quartz and feldspar of smaller size than the corresponding fragments in the sandstone matrix (Fig. 7). The intraclasts show relics of the original lamination of the microsphorite sediment. The lamination embraces thin laminae enriched in extremely fine quartz detritus. The morphology and character of internal deformation of the intraclasts suggest that they were only partly indurated during transport (Figs. 9–11). This implies that the intraclasts originated from reworking and redeposition of an original strata-bound microsphorite deposit by highly turbulent water flow. Alpha-autoradiography of ore minerals (leucoxene, U-Ti oxides) shows that they are concentrated around the intraclasts, and are also disseminated in the sandstone matrix (Figs. 14–15). Clusters of euhedral apatite in the sandstone matrix represent a younger generation of phosphate, related probably to the diagenetic cement formation (Figs. 12–13). The two generations of apatite are cut by quartz-carbonate veinlets and by sulphides (Fig. 6). The chemical composition of phosphate in intraclasts as well as in the sandy matrix cor-

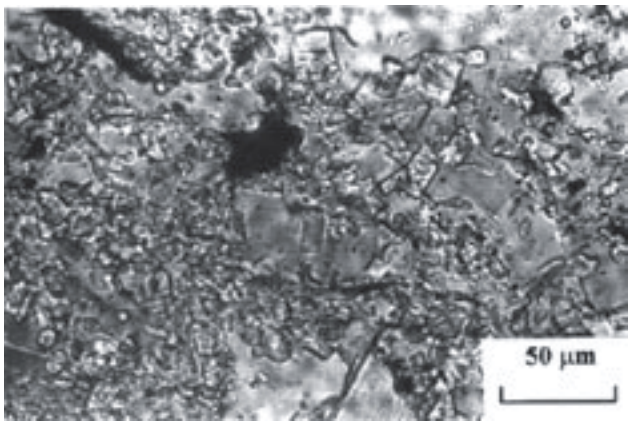

Fig. 12. Columnar and hexagonal sections of recrystallized apatite (darker with higher relief) in the sandstone matrix. Go 21, transmitted light, parallel polar.

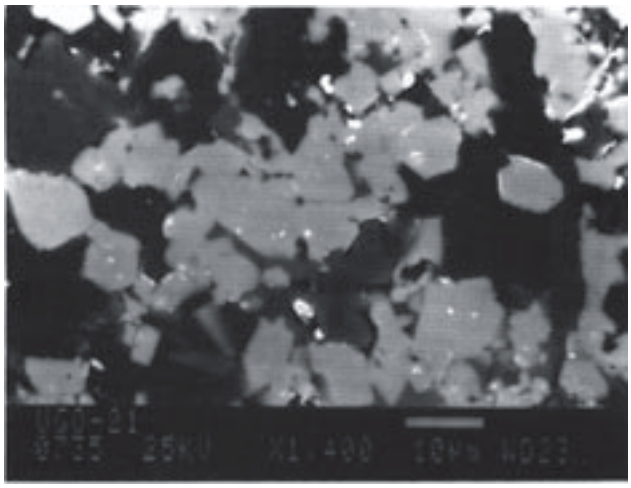

Fig. 13. Columnar and hexagonal sections of recrystallized apatite (light grey) in the sandstone matrix. Go 21, SEM-BEI.

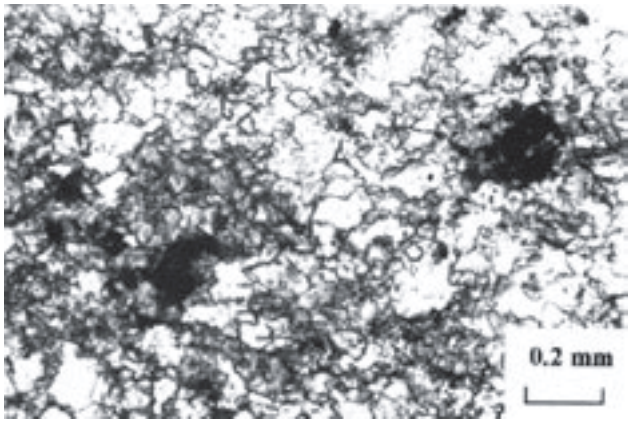

Fig. 14. Grains of U-Ti oxides (black) in the sandstone. Go 21, transmitted light, parallel polar.

responds to fluorapatite (Table 1). A well-defined empirical relation between the carbonate content and the a-cell dimension of carbonate fluorapatite (francolite), the marine variety

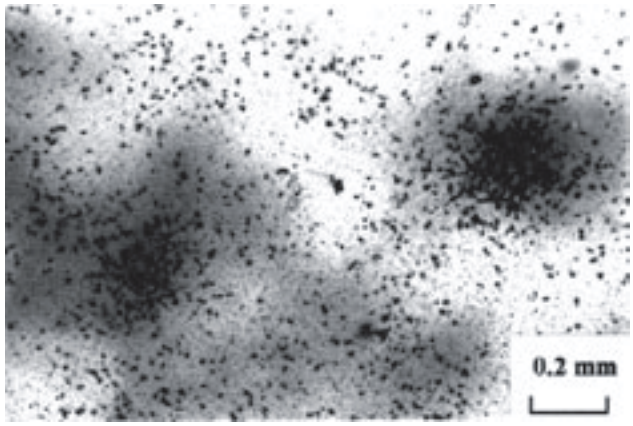

Fig. 15. α-autoradiography confirms accumulation of uranium in the grains of U-Ti oxides from Fig. 13.

Table 1: Chemical composition of apatite.

	Weight %		
Sample	Go 20	Go 21.1	Go 21.2
Ca	41	38.7	39.6
Si		0.2	0.2
Fe	0.2		
P	18.7	17.6	17.7
O	40.1	38.5	38.9
Total	100.0	95.0	96.4
	Atomic proportion (to 8)		
Ca	5.03	5.04	5.07
P	2.97	2.96	2.93

of apatite, provides a method for calculating the CO_2 content in the crystal lattice (Gulbradsen 1970 and Schuffert et al. 1990). $\Delta 2\theta_{(004)-(410)} = 1.64$ and $\Delta 2\theta_{(300)-(002)} = 7.21$ in our samples (Go 24 and Go 3/2) does not indicate carbonate-ion substitution in the fluorapatite which might be the result of metamorphic purification of the crystal structure (Table 2).

The matrix apatite is accompanied by a diagenetic to very low-grade metamorphic association of minerals represented by Fe-dolomite, uraninite, U-Ti oxides, Ti oxides, framboidal pyrite, chlorites, muscovite, and albite.

Fe-dolomite forms oval concretions up to several cm, and it also fills fissures in association with quartz and sulphides (Figs. 5–6). The Fe-dolomite is fine-grained in concretions (grains up to 50 μm), but it is coarser grained (0.2 to 0.5 mm) in veinlets (up to 1 mm thick). The chemical composition of the dolomite is shown in Table 3.

The following ore minerals occur in Gočaltovo phosphatic sandstone: uraninite, U-Ti oxides, pyrite, pyrrhotite, magnetite, marcasite, chalcopyrite, tetrahedrite, bornite, covellite, chalcocite and secondary iron hydroxides and torbernite (Melnikova 1974; Rojkovič et al. 1989b).

Uraninite forms small grains (2 to 10 μm across) concentrated at the margins of Ti-oxides. Alpha-autoradiography suggests that uraninite also rims apatite intraclasts.

Table 2: X-ray diffraction analyses of fluorapatite.

Go 24			Go3/2			Fluorapatite (Berry et al. 1974)		
2 θ	d	I	2 θ	d	I	d	I	hkl
21.87	4.062	7	21.91	4.054	11	4.055	8	200
22.91	3.878	5	22.94	3.874	10	3.872	8	111
25.86	3.443	40	25.88	3.440	34	3.442	40	**002**
29.06	3.070	15	29.10	3.066	18	3.067	18	210
31.89	2.804	100	31.95	2.802	100	2.800	100	211
32.24	2.774	40	32.25	2.773	40	2.772	55	112
33.07	2.707	50	33.09	2.704	69	2.702	60	**300**
34.12	2.626	25	34.13	2.624	23	2.624	30	202
36.54	2.457	6	36.72	2.445	3	2.517	6	301
39.48	2.281	7	39.31	2.899	6	2.289	8	212
40.01	2.252	19	40.02	2.250	27	2.250	20	310
42.47	2.127	8	42.50	2.125	3	2.140	6	311
45.39	1.997	5	45.38	1.997	6	2.061	6	113
46.86	1.937	18	46.86	1.937	26	1.937	25	222
48.23	1.886	9	48.26	1.884	15	1.884	14	312
49.56	1.838	21	49.57	1.837	30	1.837	30	213
50.73	1.798	11	50.74	1.797	16	1.797	16	321
51.53	1.772	10	51.55	1.771	14	1.771	14	**410**
52.28	1.748	8	52.28	1.748	13	1.748	14	402
53.17	1.721	13	53.19	1.721	14	1.722	16	**004**
56.09	1.638	5	56.11	1.637	7	1.637	6	322

Table 3: Chemical composition of carbonate in the sample Go 23.

Weight %			
CaO	MgO	FeO	CO_2
31.4	12.7	10.8	45.1
Atomic proportion			
Ca	Mg	Fe	Total
1.09	0.61	0.29	2.00

U-Ti oxides occur in the form of small grains up to 0.1 mm disseminated in rock. Alpha-autoradiography confirms radiation of alpha particles from isolated grains of leucoxenized ore minerals (Figs. 14–15). Their inhomogeneity observed under scanning electron microscopy as well as their chemical composition suggest that they represent intergrowths of uraninite and Ti oxides ("uranium-bearing leucoxene", Table 4).

Rutile frequently occurs as elongated and irregular grains up to 0.2 mm across showing brown and beige internal reflection and twinning lamellae in reflected light. The elongated grains often show orientation concordant to cleavage. The trellis-like texture of Ti-oxides (up to 0.1 mm) representing replacement of ilmenite by Ti-oxides in former allogenic Fe-Ti oxides is rarely observed (Fig. 16). Rare rounded grains of **magnetite** up to 40 μm are noted.

Pyrite grains (up to 10 μm) and framboidal aggregates (up to 20 μm) are disseminated in rock (Fig. 17). In Permian rocks of the Western Carpathians more abundant framboidal pyrite has been found only in the continental arkosic sandstone with abundant coalified plant remnants in the Hronic Unit of the Kozie Chrbty Mts. (Rojkovič 1997).

Chlorites are represented either by fine-grained aggregates showing preferential orientation in the matrix or by disordered aggregates in cavity fills and fine veinlets. Both types of chlorites show the same optical features and have similar chemical composition.

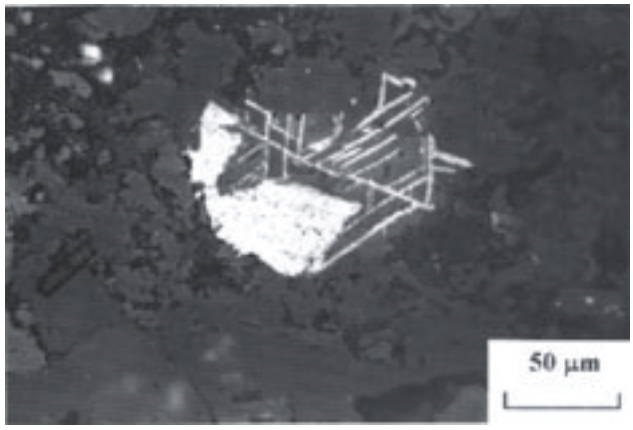

Fig. 16. Trellis of rutile (light grey) represents relict of clastic Fe-Ti oxide replacement. Go 21, reflected light, parallel polar.

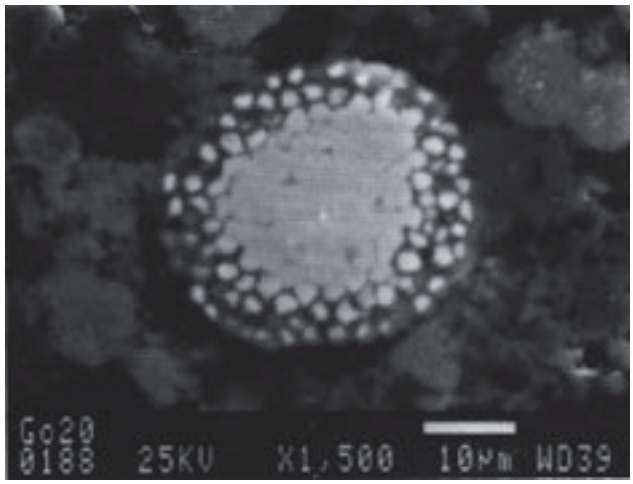

Fig. 17. Partly recrystallized framboidal aggregate of pyrite (white) in the sandstone. Go 1, SEM-SEI.

Table 4: Chemical composition of U-Ti oxides in the sample Go 20.

Weight %					
UO_2	TiO_2	Fe_2O_3	CaO	SiO_2	Total
39.4	49.6	2.0	3.1	5.8	99.9
Atomic proportion					
U	Ti	Fe	Ca	Si	O
0.48	2.05	0.08	0.19	0.32	6

The analysis of chlorite and muscovite was done in the Laboratory of electron microanalysis of the Geological Survey of Slovak Republic in Bratislava using a JEOL-733 SUPERPROBE electron microprobe. The accelerating voltage was 15 kV, the beam current 11–12 nA and the counting time 20 sec. Natural and synthetic standards were used for calibration, and a ZAF correction procedure was employed.

Table 5: Chemical composition of chlorites (in weight %).

Sample	Go3/2	Go3/2	Go4/1	Go4/1	Go4/1	Go4/1	Go2/1	Go2/1	Go2/1
SiO_2	25.74	26.48	25.63	25.40	27.99	25.83	25.03	25.86	25.99
TiO_2	0.00	0.00	0.00	0.00	0.19	0.00	0.00	0.00	0.00
Al_2O_3	22.24	20.86	20.67	22.18	22.68	21.44	21.93	21.99	21.95
FeO	22.28	20.54	20.79	21.36	18.87	20.08	20.77	20.73	20.38
MnO	0.00	0.00	0.13	0.00	0.00	0.00	0.00	0.15	0.13
MgO	16.87	17.32	17.10	16.52	15.27	16.85	16.56	17.34	17.37
CaO	0.00	0.44	0.32	0.00	0.20	0.17	0.17	0.10	0.00
Total	87.13	85.64	84.64	85.46	85.20	84.37	84.46	86.17	85.82
Atomic proportion to 28 oxygen									
Si	5.356	5.561	5.472	5.368	5.800	5.494	5.346	5.402	5.438
Al	2.644	2.439	2.558	2.632	2.200	2.506	2.654	2.598	2.562
Al	2.808	2.726	2.644	2.892	3.340	2.868	2.868	2.817	2.850
Ti	0.0	0.0	0.0	0.0	0.029	0.0	0.0	0.0	0.0
Fe	3.877	3.608	3.712	3.775	3.271	3.571	3.711	3.622	3.567
Mn	0.0	0.0	0.024	0.0	0.0	0.0	0.0	0.027	0.023
Mg	5.232	0.100	5.443	5.203	4.717	5.341	5.274	5.401	5.416
Ca	0.0	5.423	0.074	0.0	0.044	0.039	0.038	0.022	0.0
MF*	0.42	0.40	0.40	0.42	0.41	0.40	0.41	0.40	0.40

*MF = Fe/Fe + Mg

The studied chlorites belong to the Mg-Fe chlorite group (Table 5). They contain more Fe than Mg, and consequently show a negative optical character. The dark colour of the chlorites as well as their distinct pleochroism points to the prevailing content of Fe over Mg. According to the commonly used classification of Hey (1954), the composition of the chlorites corresponds to trioctahedral chlorite of thuringite group (calculated on the basis of 28 oxygens). The chlorites contain 5.35 to 5.56 Si atoms and have a Fe/(Fe+Mg) ratio of 0.39 to 0.42 with Fe_{TOT} of 3.57 to 3.77. This is within the range of ripidolite. Subordinate chlorite with higher content of Fe belongs to the chamosite group. The content of 5.66 to 5.80 Si atoms and ratio Fe/(Fe+Mg) of 0.38 to 0.41 is within the range of picnochlorite.

Muscovite forms aggregates of fine oriented scales, which are bent by crenulation cleavage in some places. The clastic micas can be distinguished from the neoformed muscovite by their shape and distinctly larger size. They are irregularly disseminated within the rock fabric and show secondary alteration features at their margins. Chemical analysis (Table 6) indicates the dioctahedral character, with a content of 6.1 to 6.4 Si atoms and approximately 4 (4.06–4.2) ions in Y position (calculated on the basis of 22 oxygen atoms). The composition of the analysed muscovite is characterized by (Mg, Fe) of 0.33 to 0.47 and Al_{TOT} of 5.4 to 5.6. The Si/Al ratio in tetrahedral component is greater than 6:2. This is equilibrated by substitution of Al by bivalent ions in octahedral component. The dominant interlayer cation in X position is K, with a subordinate contribution of Na and Ca (with more than 1.7 atoms).

Albite is represented by xenomorphic grains often without twinning. Its chemical composition is close to pure albite (99 mol. % of albite component and 1 % of anortite plus orthoclase component).

A younger generation of pyrite, pyrrhotite, chalcopyrite and marcasite in carbonate and quartz-carbonate veinlets represents a hydrothermal association of minerals. **Carbonate** grains up to 0.5 mm form aggregates and veinlets showing pressure twinning in the reflected light. Xenomorphic grains of **pyrrhotite** (0.05 to 0.2 mm in size) forming aggregates up to 2 mm occur in close association with **chalcopyrite** (0.1 to 0.5 mm) which encloses euhedral pyrite (Fig. 18). Euhedral grains of **marcasite** (up to 5 μm) rim and replace pyrrhotite.

Table 6: Chemical composition of muscovite (in weight %).

Sample	Go3/2	Go3/2	Go4/1	Go4/1	Go4/1
SiO_2	45.66	46.60	48.10	45.67	44.71
TiO_2	0.27	0.65	0.32	0.30	0.28
Al_2O_3	35.58	34.88	33.19	33.48	35.07
FeO	1.45	0.72	1.37	1.19	1.44
MgO	1.06	1.29	0.89	1.66	1.52
CaO	0.24	0.00	0.00	0.00	0.00
Na_2O	0.86	0.82	0.46	0.00	0.00
K_2O	8.80	9.27	8.90	10.51	9.84
Total	93.92	94.23	93.23	92.81	92.86
Atomic proportion to 22 oxygen					
Si	6.121	6.200	6.454	6.235	6.089
Al	1.879	1.800	1.546	1.765	1.911
Al	3.741	3.691	3.703	3.622	3.713
Ti	0.027	0.066	0.032	0.031	0.028
Fe	0.162	0.080	0.154	0.136	0.164
Mg	0.212	0.256	0.178	0.337	0.308
Ca	0.035	0.0	0.0	0.0	0.0
Na	0.223	0.211	0.121	0.0	0.0
K	1.505	1.580	1.523	1.830	1.710
(Fe.Mg)	0.37	0.34	0.33	0.47	0.47

Goethite and torbernite are products of supergenic alteration. **Goethite** forms colloform and zoned aggregates up to several mm in size. Pseudomorphs of goethite replacing pyrite crystals and framboidal pyrite are common. **Torbernite** scales (from 10 to 20 μm across) are disseminated in sandstone as well as in the apatite intraclasts (Fig. 19). They rim phosphorite intraclasts and form veinlets (up to 20 μm thick) filling fissures of the rock. Green internal reflection in reflected light is characteristic.

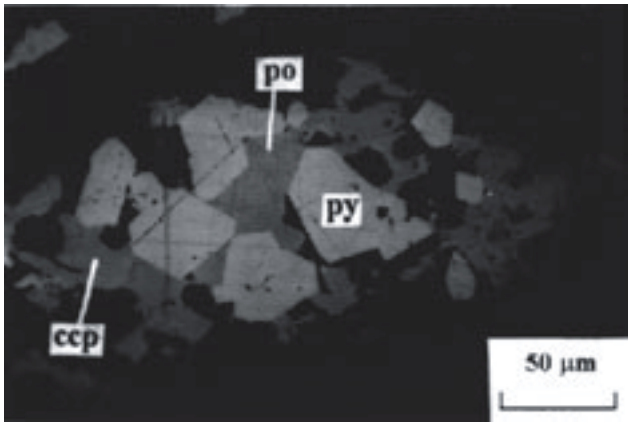

Fig. 18. Crystals of pyrite (py) in pyrrhotite (po) and chalcopyrite (ccp). Go 5, reflected light, parallel polar.

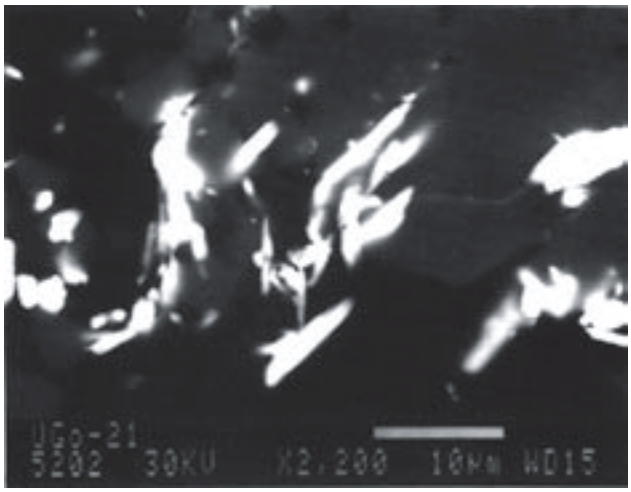

Fig. 19. Torbernite scales (white) in the margin of phosphorite intraclast (grey) and in the quartz (black). Go 21, SEM-BEI.

Grade of metamorphism

The assemblage of metamorphic minerals represented by muscovite–chlorite–albite is very constant through a broad temperature range, from the latest stage of diagenesis to a very low- and low-grade of metamorphism. It is indicated by the presence of high-aluminium Fe-chlorite, which is characteristic of Al-Fe rich protolith. These trioctahedral chlorites contain 12 cations in octahedral component on the basis $O_{20}(OH)_{16}$ and an approximately equal content of Al in both (tetrahedral and octahedral) components.

The chlorites represent a group of minerals of variable composition reflecting the chemical conditions of their origin. Cathelineau (1988) demonstrated the application of a chlorite geothermometer based on the Al^{IV} content of chlorite in hydrothermally altered andesite. An increase in Fe^{VI} and decrease in the octahedral vacancy accompanies this change. Al↔Si and Fe↔Mg substitutions in chlorite reflect changes not only in temperature (Kranidiotis & MacLean 1987) but also in the oxygen and/or sulphur fugacity of the coexisting fluids (Walshe 1986; Bryndzia & Scott 1987). Several calculations of the chlorite geothermometry were based on these series of linear relations (Cathelineau & Nieva 1985; Cathelineau 1988; Jowett 1991; Zang & Fyfe 1995). The temperatures of the studied chlorites, calculated on the basis of several methods, vary in the range from 250 to 366 °C (Table 7).

Methods taking into account X_{Fe} gave higher temperature than those using only Al^{IV}. The differences in temperature are about 60 °C calculated in the single chlorite pairs by the different methods. The empirical models of Cathelineau & Nieva (1985) and Zang & Fyfe (1995) indicate maximum temperatures lower than 300 °C (around 250 to 290 °C), which correspond to very low-grade metamorphism. The wide range of the calculated temperatures may reflect insufficient equilibrium of coexistent chlorite pairs. No geothermometer includes the whole range of natural conditions with different temperatures, coexisting mineral phases, Fe/(Fe+Mg), oxygen fugacity etc.

The associated muscovite belongs to low Na-bearing white mica with Na/(Na+K) values from 0 to 0.12 mol. %. Negligible Na↔K substitution has no effect on *a* and *b* cell dimensions. The chemical composition of muscovite has been used for numerical calculation of b_0 values and the following geobarometric estimations according to the method proposed by Guidotti et al. (1989). The average b_0 value calculated on the basis of Σ(Fe+Mg), ΣAl and Si content atoms reaches 0.9009 nm (n = 13 and standard deviation = 0.0006 nm). Guidotti & Sassi (1986) compared this value to the boundary between the low- and medium-grade of regional metamorphism based on the division of the metamorphic series in the sense of Miyashiro (1961). It corresponds to data from the Barrowian metamorphic terrain, which is well described from Scotland (Fettes et al. 1976).

The climax of regional metamorphism of the Štítnik Formation sediments cannot be estimated precisely due to the very broad stability field of the chlorite-muscovite-albite assemblage. The illite crystallinity indicates temperatures from 200 to 250 °C (Šucha & Eberl 1992), which correspond to the minimum temperatures calculated according to the chlorite geothermometry.

Table 7: Temperatures calculated according to different chlorite geothermometers.

Cathelineau & Nieva (1985)	Cathelineau (1988)	Jowett (1991)	Zang & Fyfe (1995)
299.5 °C	363.7 °C	366 °C	290.8 °C
272.5 °C	330.6 °C	332.6 °C	270.9 °C
289.8 °C	349.7 °C	350.6 °C	286.3 °C
298.7 °C	361.8 °C	364.2 °C	289.6 °C
251.8 °C	292.2 °C	283.2 °C	244.6 °C
284.4 °C	341.6 °C	343.5 °C	278.1 °C
300.1 °C	365.2 °C	367.3 °C	292.7 °C
290.3 °C	350.5 °C	352.3 °C	284.3 °C
294.1 °C	356.3 °C	358.1 °C	287.8 °C

Geochemistry of phosphatic sandstone

The major and minor elemental analysis of the phosphatic sandstone reveals very distinct enrichment in CaO (15 to 28 weight percent) and P_2O_5 (12 to 18 weight percent), which reflects the abundance of apatite and Fe-dolomite. Higher loss of ignition (LOI), from 3 to 7 weight percent is mainly due to loss of CO_2 during ignition of Fe-dolomite (Table 8).

The trace element analysis of the sandstone shows increased uranium content and moderately increased lead content. Concentration of these elements confirms the presence of uranium mineralization in the study sequence (Table 9). Increased concentration of copper could be correlated to chalcopyrite and, to a lesser extent, to torbernite. Phosphatic sandstone near Gočaltovo contains up to 500 ppm of REE and up to 250 ppm Y (Table 10). The nature of distribution of REE and Y in the rock paragenesis remains unknown, though we presume that they are bound to apatite and uranium minerals. Earlier results suggested the presence of slight negative Ce anomaly in the phosphatic sandstone (Rojkovič 1997). However, the detailed AAS-ICP analysis done for the purpose of this study revealed no negative Ce anomaly in the phosphatic sequence (Fig. 20).

Table 8: Chemical composition of rocks.

Sample	Go 5	Go 7	Go 9	Go 15	Go 21	Go 24	Go 24a
SiO_2	32.42	73.40	59.81	75.76	36.83	48.24	45.17
TiO_2	0.60	0.60	0.96	0.70	0.55	0.47	0.80
Al_2O_3	8.58	12.05	15.42	12.04	7.89	10.37	9.69
Fe_2O_3	1.01	1.22	2.39	2.50	0.85	3.32	2.32
FeO	1.53	1.95	2.26	0.58	1.87	0.68	0.66
MnO	0.073	0.010	0.030	0.12	0.185	0.240	0.274
MgO	1.77	3.72	2.82	0.98	3.10	1.57	1.48
CaO	28.42	0.23	2.32	0.30	22.9	14.89	18.02
Na_2O	1.70	1.42	2.49	1.60	2.97	3.80	3.68
K_2O	1.12	2.75	4.77	2.91	0.69	0.94	0.58
P_2O_5	17.92	0.10	0.18	0.13	13.74	12.04	13.48
LOI	4.89	1.77	6.14	1.99	7.41	2.78	3.41
H_2O-	0.13	0.30	0.34	0.72	0.16	0.64	0.26
Total	100.16	99.52	99.93	100.33	99.15	99.98	99.82
rock	sandstone	shale	shale	sandstone	sandstone	sandstone	sandstone

Table 9: Trace elements in rocks (in ppm).

Sample	Go 5	Go 5a	Go 7	Go 9	Go 13	Go 15	Go 21	Go 21a	Go 24	Go 24a
B	182	173	140	243		205	110	129	115	133
Ba		39						37	172	
Co	50	51	13	7	11	4	32	46	35	46
Corg	1800		900	1800	1000	600	1800		2100	
Cu	65	70	15	5	47	17	135	110	275	156
La	59	77	10	17		10	48	76	93	60
Mo	3	1.5	1	2	2	1	3	3.4	3.3	8.2
Ni	26	28	18	37	35	18	20	26	22	27
Pb	42	53	8	8	16	8	115	110	127	153
Sr		1010						252	160	193
Th			12.40	13.10	21	11.70	75.40			
Ti	1590	1990	3300	5250	5900	3600	2510	3320	2630	3350
U	970		33	112	80	35.9	2140		1540	
V	35	57	33	69	74	28	33	66	69	58
Zr	620	573	340	263	470	400	320	317	385	366
Y	209	190	24	33	39	27	110	149	260	431
Yb	9.8	18.5	1.3	1.7		1.7	4.8	13.9	37	58.5
rock*	sandst.	sandst.	shale	shale	sandst.	sandst.	sandst.	sandst.	sandst.	sandst.

*sandst. = sandstone

Table 10: Rare earth elements in sandstones (in ppm).

Sample	Go 2	Go 5	Go 21a	Go 24	Go 24a
La	47.00	63.00	60.00	58.00	61.00
Ce	84.00	128.00	120.00	177.00	120.00
Pr	7.00	30.00	25.00	50.00	25.00
Nd	37.00	92.00	55.00	47.00	74.00
Sm	12.00	30.20	17.90	30.00	27.00
Eu	1.06	1.74	1.01	3.00	1.80
Gd	7.20	51.40	27.80	23.00	35.00
Tb	0.00	5.65	3.70	7.60	8.13
Dy	12.50	25.60	7.30		28.90
Ho	0.06	3.52	2.01	9.90	4.93
Er	4.90	17.90	10.70		33.20
Tm	0.37	2.50	3.55	5.20	5.50
Yb	8.80	22.50	11.20	42.60	44.00
Lu	1.09	3.80	2.40	6.30	5.40
Y	60.00	173.00	105.00		251.00

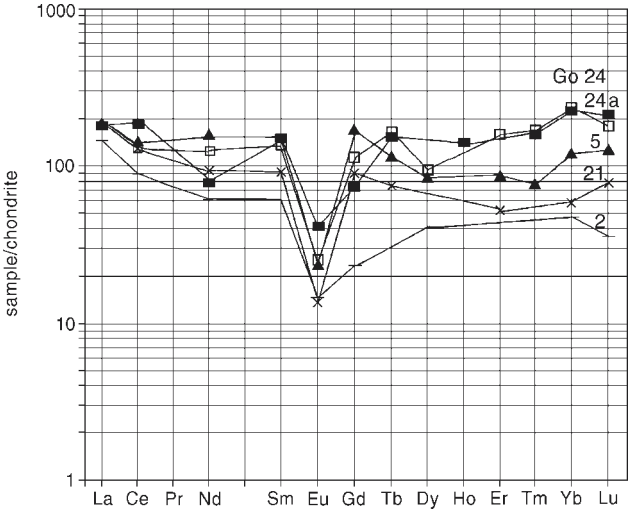

Fig. 20. Distribution of the rare earth elements in the sandstone from Gočaltovo.

Discussion

Phosphatic sediments of the Štítnik Formation represent a part of transgressive sequence reflecting transition from the continental to the sabkha-lagoonal sedimentary regimes (Fig. 21). The following lithofacial features were observed:

1. gradual development of the Štítnik Formation from the coarse-grained continental Rožňava Formation;

2. distinct upward decrease of grain-size in siliciclastic sediments and transition to lagoonal terrigenous-carbonate facies in the upper part;

3. rapid vertical changes of lithology, which are well documented in the phosphorite-bearing sequence.

The redeposition of phosphorite clasts indicates abrupt changes of the paleoenvironment, from a low-energy phosphogenic regime to a high-energy regime strongly influenced by traction flows of fluvial distributary channels.

The main argument supporting the idea of continental origin of these phosphatic sediments is the absence of marine fauna. Moreover Šuf (1963) has found fresh-water bivalve tests of the species *Carbonicola*. On the basis of this fact and on the observed sedimentological features, we interpret the Štítnik Formation phosphatic sediments as lacustrine deposits. Cyclic alternation of sandstone and shale with well-developed bedding is a typical feature. The shale contains sandy laminae and considerable amounts of silt detritus. The sandstone shows massive structure with moderate sorting, and represents traction flow sediment. Sorting ranges from 0.5 to 1.0 φ according to the visual scale of Folk (1974). The moderate sorting of lenticular sandstone bodies is the result of deposition in river distributary channels which advanced into the lacustrine basin. These sediments contain phosphorite intraclasts and shale clasts. Rapid influx of clastic detritus and sudden progradation of detrital material into the lacustrine domain was associated with down-slope redeposition by a system of flows, similar to turbidite currents. This sedimentary process is documented by graded bedding of the sandstone. The fine-grained, horizontally laminated sediments indicate a low energy sedimentary realm.

Lacustrine phosphorite represents a unique type of phosphate accumulation. Concentration of phosphate minerals was described in recent eutrophic lakes (Kleeberg & Dudel 1997; Penn & Auer 1997) as well as in oligotrophic lakes (Lake Baikal, Callender & Granina 1997). Phosphate minerals were also reported from the Upper Carboniferous coaly "tonsteins" associated with limnic coal-bearing facies (Różkowska 1990; Stadler & Werner 1962; Burger et al. 1997). A characteristic feature of recent eutrophic lakes is a low content of oxygen and high content of nutrients. They are shallow (up to 18 m), transparent only over a few meters of water column, and their drainage area has flat relief. The interpretation of a continental origin for the phosphatic sediments in the Štítnik Formation is based on the absence of any faunal assemblages. Abundant fauna is typical of shallow water marine phosphates as well as in the associated sediments. Sedimentary features of the Štítnik Formation indicate a high-energy depositional regime. Redeposited intraclasts of phosphorite showing in places plastic deformation are here commonly observed. The clasts of phosphorite are mostly structureless and cryptocrystalline. The remnants of the original lamination can be seen in some clasts. Inclusions of fine-grained siliciclasts are common. However, the origin of the investigated primary phosphates can hardly be documented with certainty because of considerable post-depositional alteration of the sequence.

Rivers supplied particulate phosphorus from weathered rocks. Continental weathering is the most important source of phosphorus. Föllmi (1995) described the high dependence of the total phosphorus flux rate on total and chemical continental weathering. Coupling processes between climate and continental weathering (changing from a high rate of total weathering to prevalent chemical weathering) controlled this mechanism. Several authors (e.g. Fox et al. 1986, the modern Amazon estuary) described phosphorus enrichment in modern rivers and estuaries. The original phosphate deposit was formed in a freshwater anoxic basin with high microbial activity.

The depositional model of the Štítnik Formation assumes sedimentation in a relatively flat drainage area with occurrences of limnic ponds (Vozárová & Vozár 1988). The phosphorus was bound to iron hydroxides during transport and it

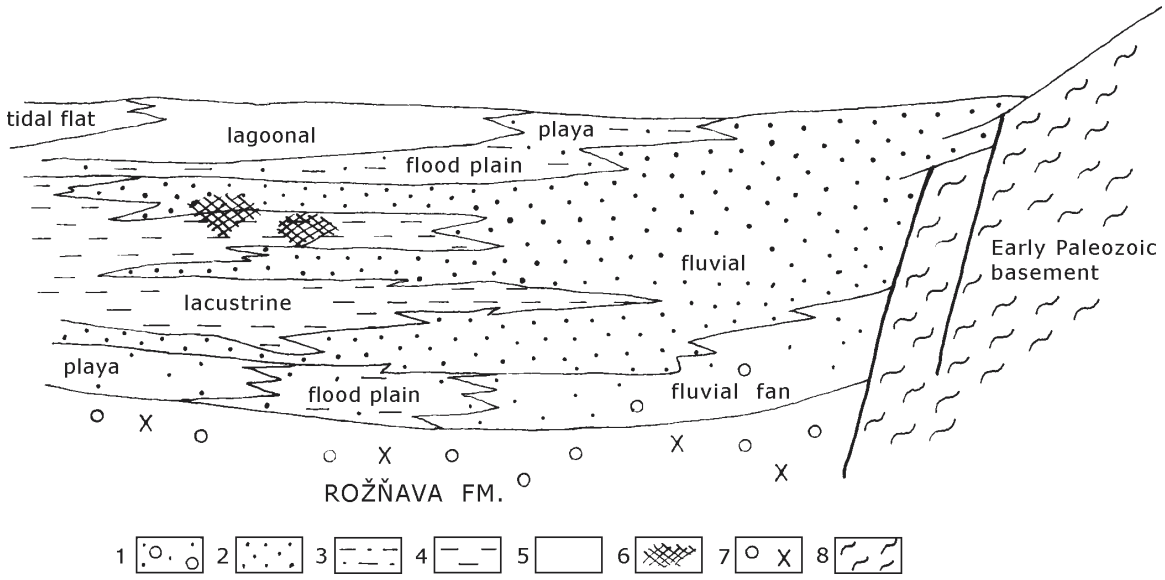

Fig. 21. Facies section of the Štítnik Formation sedimentary basin. *Explanations:* **1** — sandstone with subordinate conglomerate intercalations, **2** — sandstone lithofacies, **3** — siltstone, mudstone, shale with intercalations of sandstone, locally sandy turbidite, **4** — shale with subordinate intercalations of siltstone and fine-grained sandstone, **5** — dolomite, "dedolomite", shale, **6** — phosphatic sandstone, **7** — sediments of the Rožňava Formation, **8** — rock complexes of the Early Paleozoic basement.

was released by reduction in suboxic/anoxic bottom water or in the sediment pore waters. This mechanism was described from shallow marine and deltaic sedimentary systems (Berner 1973; Krom & Berner 1981 and de Lange 1986).

Apatite precipitated most probably within the topmost part of an organic-rich sediments column, as a result of complex phosphorus transformations in the interface environment. The common association of framboidal pyrite and apatite suggest that the precipitation took place in the upper part of anoxic sulphidic diagenetic zone and was accompanied by intense degradation of organic matter. The sediments in most eutrophic lakes are enriched in organic sulphur (Urban et al. 1999). Sedimentary formation of pyrite is consistent with anoxic conditions at the sediment-water interface, the deposition of organic-rich sediments, and severe eutrophication (Manning et al. 1999). Pyrite framboid formation is considered to be a consequence of greigite formation in weakly reducing conditions spatially linked to redox interfaces (Wilkin & Barnes 1997).

The presence of Fe-chlorite suggests the existence of a thin suboxic diagenetic zone in surface sediment. Precipitation of the phosphates could also be affected by the composition of detritus, which was locally extremely rich in felsic rhyolite material. Volcaniclastic detritus was poor in Na, K, Ca, Mg ions, and, on the contrary, enriched in P. However, aggressive acid waters of eutrophic lakes decomposed volcaniclastic detritus resulting in the increased water alkalinity. A sufficient Ca content enabled the formation of microsphorite, most probably under microbial control. Bacterial concentration of dissolved phosphate could also lead to precipitation of apatite due to concentration/release cycles associated with oscilation of the suboxic/anoxic interface (Gächter & Meyer 1993). Free Na ions could be adsorbed by clay minerals, which were most probably represented by smectite. This suggests complex and multi-stage origin of the Štítnik Formation phosphatic sediments.

The observed sedimentary structures and the evidence of phosphorite redeposition allow us to suggest recurrent changes in the phosphogenic environment, in which traction flows affected distribution of phosphatic particles and their mixing with siliciclastic sediments. This process might reflect water-level fall, during which river systems invaded the lacustrine environment, and, in extreme cases, caused down-slope transport of detrital phosphorite. A flat drainage area could be suggested by the absence of coarser-grained clastic sediments (conglomerate and coarse-grained sandstone). Redeposition of phosphorite clasts could also occur due to high-energy events, like storms. This process could lead to disturbance of the water column stratification and to the mixing of anoxic bottom water with oxygenated water resulting in further adsorption of phosphorus by ferric iron.

The secondary stage of phosphate precipitation occurred during later stages of diagenesis. Apatite precipitated from anoxic pore waters to form cement between siliciclastic grains as well as thin rims around the microsphorite intraclasts. The precipitation of apatite was accompanied by formation of Fe-chlorite. During diagenesis, smectite was replaced by illite, the excess sodium was bound in albite, and uranium was adsorbed by phosphorite intraclasts. The subsequent very low-grade metamorphism affected the recrystallization of microsphorite and the formation of a chlorite-albite-muscovite assemblage from diagenetic chlorite and smectite. Alpine hydrothermal processes have contributed to the formation of quartz-carbonate veinlets with sulphides that cut phosphorite intraclasts as well as apatite aggregates in cement. The products of supergene processes are iron hydroxides and torbernite.

Summary

The sandstone facies of the Štítnik Formation contains intraclasts of microsphorite and small crystals of apatite in the matrix. Apatite is accompanied by uranium mineralization, which is represented by uraninite and U-Ti oxides. Pyrite, pyrrhotite, marcasite, and chalcopyrite occur in quartz-carbonate veinlets. The phosphatic sandstone shows distinct enrichment in phosphorus (up to 18 weight percent P_2O_5), reflecting abundance of apatite. The total REE content is moderately high, with maximum up to 500 ppm and Y up to 250 ppm.

The phosphatic sandstones in the Štítnik Formation reflect phosphogenesis in a lacustrine environment that was invaded and destroyed by fluvial systems. Finely laminated shales and siltstones, commonly interlayered with thin turbidite sandstones represent the lacustrine part of the sequence. The fine-grained sediments show abrupt facies changes towards a belt of fluvial distributary channel sandstones and channel fills. Sedimentary structures indicate recurrent changes of the environment dynamics, from low to high-energy conditions. Intraclasts of microsphorite in the sandstone are interpreted to be the result of reworking and winnowing of original strata-bound phosphate deposits formed in an organic carbon-rich eutrophic lake. Phosphorus was concentrated in this environment as a result of riverine supply of particulate P phases as well as phosphate sorbed on ferric iron compounds. Under anoxic conditions, phosphorus was liberated into the pore waters of lacustrine sediment and aided the precipitation of apatite. This iron redox pump mechanism was microbially controlled and concentrated phosphorus in a thin suboxic and in the upper part of an anoxic sulphidic diagenetic zone in organic-rich lacustrine sediments.

Subsequent diagenetic to very low-grade metamorphic processes caused recrystallization of the primary apatite and formation of the associated minerals, including Fe-dolomite, chlorite, muscovite, albite. During this process phosphates adsorbed U, Y, REE, Cu and Pb. The Alpine hydrothermal processes mobilized disseminated elements and concentrated them into the sulphides of quartz-carbonate veinlets.

Acknowledgements: The study was partly supported by Grant 1/4090/97 of VEGA. We thank Ľ. Puškelová from Geological Institute of Slovak Academy of Sciences, J. Kubová from Faculty of Science of Comenius University and P. Konečný from Geological Survey of the Slovak Republic for the analyses of some of the rocks and minerals. This manuscript benefited greatly from the reviews of K.P. Krajewski, Z. Kukal and M. Mišík.

References

Bajaník Š., Vozárová A. & Reichwalder P. 1981: Lithostratigrafic classification of Rakovec Group and Late Paleozoic in the Spišsko-gemerské rudohorie Mts. *Geol. Práce, Spr.* 75, 27–56 (in Slovak).

Berner R.A. 1973: Phosphate removal from seawater by adsorption on volcanic ferric oxides. *Earth Planet. Sci. Lett.* 18, 77–86.

Berry L.G. (Ed.) 1974: Joint Committee on powder diffraction standards. Selected powder diffraction data for minerals. Philadelphia, 1–833.

Bryndzia L.T. & Scott S.D. 1987: The composition of chlorite as a function of sulfur and oxygen fugacity: An experimental study. *Amer. J. Sci.* 287, 50–76.

Burger K., Gabzdyl W. & Ryszka J. 1997: Phosphorus concentration in limnic deposits of Silesian Formation (Upper Carboniferous) in the Upper Silesian coal basin. *Prace Państw. Inst. Geol.* CL VII, 313–317 (in Polish).

Bystrický J. & Fusán O. 1955: About the age of sandstone formation in the Štítnik area. *Věst. ÚÚG* 30, 135–153 (in Slovak).

Callender E. & Granina L. 1997: Biogeochemical phosphorus mass balance for Lake Baikal, southeastern Siberia, Russia. *Mar. Geol.* 139, 5–19.

Cathelineau M. 1988: Cation site occupancy in chlorites and illites as a function of temperature. *Clay Miner.* 32, 471–485.

Cathelineau M. & Nieva D. 1985: A chlorite solution geothermometer. The Los Azufres (Mexico) geothermal system. *Contr. Mineral. Petrology* 91, 235–244.

DeLange G.J. 1986: Early diagenetic reaction in interbedded pelagic and turbidic sediments in the Nares Abyssal Plain (western North Atlantic): Consequences for the composition of sediment and interstitial water. *Geochim. Cosmochim. Acta* 50, 2543–3180.

Fettes D., Graham C.W., Sassi F.P. & Scolari A. 1976: The lateral spacing of potassic white micas and facies series variation across the Caledonides. *Scott. J. Geol.* 12, 227–236.

Folk R.L. 1962: Spectral subdivision of limestone types. In: Ham W.E. (Ed.): Classification of Carbonate Rocks. *Amer. Assoc. Petrol. Geol. Mem.* 1, 62–84.

Folk R.L. 1974: Petrology of Sedimentary rocks. *Hemphill,* Austin, Texas, 1–159.

Fox L.E., Sager S.L. & Wofsy S.C. 1986: The chemical control of soluble phosphorus in the Amazon estuary. *Geochim. Cosmochim. Acta* 50, 783–794.

Föllmi K.B. 1995: 160 m.y. record of marine sedimentary phosphorus burial: Coupling of climate and continental weathering under greenhouse and icehouse conditions. *Geology* 23, 9, 859–862.

Fusán O. 1959: Remarks to the Late Paleozoic of Gemerides. *Geol. Práce, Zoš.* 55, 171–181 (in Slovak).

Gächter R. & Meyer J.S. 1993: The role of microorganisms in mobillization and fixation of phosphorus in sediments. *Hydrobiologia* 253, 103–121.

Guidotti Ch. & Sassi F.P. 1986: Classification and correlation of metamorphic facies series by means of muscovites *b* data from low-grade metapelites. *Neu. Jb. Mineral., Abh.* 153, 363–380.

Guidotti Ch., Sassi F.P. & Blencoe G. 1989: Compositional controls on the *a* and *b* cell dimension of $2M_1$ muscovite. *Eur. J. Mineral.* 1, 71–84.

Gulbrandsen R.A. 1970: Relation of carbon dioxide content of apatite of the Phosphoria Formation to regional facies. *U.S. Geol. Survey Prof. Pap.* 700-B, B9-B13.

Hey M.H. 1954: A new rewiev of the chlorites. *Mineral. Mag.* 30, 277–292.

Jowett E.C. 1991: Fitting iron and magnesium into the hydrothermal chlorite geothermal geothermometer. *Geol. Assoc. Canada/Miner. Assoc. Canada/Soc. Econ. Joint Ann. Meeting. Toronto 1991,* Abstracts 16, A62.

Kleeberg A. & Dudel G.E. 1997: Changes in extent of phosphorus release in a shallow lake (Lake Grosser Muggelsee; Germany, Berlin) due to climatic factors and load. *Mar. Geol.* 139, 61–75.

Kranidiotis P. & MacLean W.H. 1987: Systematics of chlorite alteration at the Phelps Dodge massive sulfide deposits, Matagami, Quebec. *Econ. Geol.* 82, 1898–1911.

Krom M.D. & Berner R.A. 1981: The diagenesis of phosphorus in a nearshore marine sediment. *Geochim. Cosmochim. Acta* 45, 207–216.

Maheľ M. 1986: Geology of the Czechoslovak Carpathians. 1. Paleoalpine units. *VEDA*, Bratislava, 1–503 (in Slovak).

Manning P.G., Prepas E.E. & Serediak M.S. 1999: Pyrite and vivianite intervals in the bottom sediments of eutrophic Baptiste Lake, Alberta, Canada. *Canad. Mineralogist* 37, 593–601.

Melnikova A.M. 1974: Short characteristic of mineral composition in uranium occurrences in the Permian sediments of the Považský Inovec Mts. and Gočaltovo. *Manuscript*, *URANPRES,* Spišská Nová Ves, 1–47 (in Russian).

Mello J., Elečko M., Pristaš J., Reichwalder P., Snopko L., Vass D. & Vozárová A. 1996: Geological map of the Slovak karst 1:50,000. *Geol. Survey of the Slovak Republic*, Bratislava.

Mello J., Elečko M., Pristaš J., Reichwalder P., Snopko L., Vass D., Vozárová A., Gaál Ľ., Hanzel V., Hók J., Kováč P., Slavkay M. & Steiner A. 1997: Explanations to geological map of the Slovak Karst 1:50,000. *Geol. Survey of the Slovak Republic*, Bratislava, 1–255 (in Slovak).

Mello J., Reichwalder P. & Vozárová A. 1998: Bôrka Nappe: high-pressure relic from the subduction-accretion prism of the Meliata Ocean (Inner Western Carpathians, Slovakia). *Slovak Geol. Mag.* 4, 4/98, 261–274.

Miškovic J. & Varček C. 1983: Mineralized concretions as characteristic feature of the Gemeric Permian. In: *Vplyv geologického prostredia na zrudnenie. Geol. Úst. D. Štúra*, Bratislava, 235–243 (in Slovak).

Miyashiro A. 1961: Evolution of metamorphic belts. *J. Petrology* 2, 277–311.

Penn M.R. & Auer M.T. 1997: Seasonal variability in phosphorus speciation and deposition in a calcareous, eutrophic lake. *Mar. Geol.* 139, 47–59.

Planderová E. 1980: New data on the age of the Rožňava – Železník Group. *Geol. Práce, Spr.* 74, 113–119 (in Slovak).

Reichwalder P. 1973: Geology of the Late Paleozoic in SE part of the Spišsko-gemerské Rudohorie Mts. *Západ. Karpaty, Sér. Mineral., Petrogr., Geochém., Metalogen.* 18, 99–141 (in Slovak).

Rojkovič I. 1997: Uranium mineralization in Slovakia. *Acta Geol. Univ. Comen., Monogr. Ser.* 1–117.

Rojkovič I., Medveď J., Pošta S., Sulovský P. & Walzel E. 1989a: Rare earths from uranium mineralization occurrences in the Permian of the Gemericum, the Western Carpathians. *Geol. Zbor. Geol. Carpath.* 40, 453–469.

Rojkovič I., Šucha V., Uher P. & Franců J. 1989b: Mineralogical-geochemical characteristic of the uranium mineralization in the Permian of Gemericum. *Manuscript*, *Geologický ústav CGV SAV*, Bratislava, 1–349 (in Slovak).

Różkowska A. 1990: Content of phosphorus in coal from Upper Silesian Coal Basin. *Kwart. Geol.* 34, 4 (in Polish).

Schuffert J.D., Kastner M., Emanuelle G. & Jahnke R.A. 1990: Carbonate-ion substitution in francolite: A new equation. *Geochim. Cosmochim. Acta* 54, 2323–2328.

Stadler G. & Werner H. 1962: Ein Phosphatmineral der Crandallit Gruppe in den Kaolintongesteinen des Ruhrkarbons. *Fortschr. Geol. Rheinl. Westf.* 3, 2.

Štimmel I. 1967: Preliminary report on survey mining of adit 33 in

Gočaltovo. *Manuscript, URANPRESS,* Spišská Nová Ves, 1–7 (in Slovak).

Šucha V. & Eberl D.D. 1992: Postsedimentary alteration of the Permian sediments in the northern Gemericum and Hronicum of the Western Carpathians. *Miner. Slovaca* 24, 399–405 (in Slovak).

Šuf J. 1963: Report on geological survey in Štítnik. *Geol. Práce, Spr.* 27, 63–68 (in Czech).

Tréger M. 1973: Occurrence of uranium-bearing phosphates in the Spišsko-gemerské Rudohorie Mts. *Miner. Slovaca* 5, 61–64 (in Slovak).

Turan J. & Vančová L. 1983: Occurrences of mineralized concretions in the Permian of Gemericum. In: Vplyv geologického prostredia na zrudnenie. *Geol. Úst. D. Štúra*, Bratislava, 269–270 (in Slovak).

Urban N.R., Ernst K. & Bernasconi S. 1999: Addition of sulfur to organic matter during early diagenesis of lake sediments. *Geochim. Cosmochim. Acta* 63, 837–853.

Vozárová A. & Vozár J. 1988: Late Palaeozoic in West Carpathians. *Geol. Úst. D. Štúra,* Bratislava, 1–314.

Walshe I.L. 1986: A six-component chlorite solid solution model and the conditios of chlorite formation in hydrothermal and geothermal systems. *Econ. Geol.* 81, 681–703.

Wilkin R.T. & Barnes H.L. 1997: Formation processes of framboidal pyrite. *Geochim. Cosmochim. Acta* 61, 323–339.

Zang T. & Fyfe W.S. 1995: Chloritisation of the hydrothermally altered bedrock at the Igarape Bahia gold deposits, Carajas, Brasil. *Mineralium Deposita* 30, 30–38.